Anomalous Roughening in Experiments of Interfaces in Hele-Shaw Flows with Strong Quenched Disorder

Jordi Soriano,* Jordi Ortín, and A. Hernández-Machado

Departament d'Estructura i Constituents de la Matèria
Universitat de Barcelona, Av. Diagonal, 647, E-08028 Barcelona, Spain

(Dated: February 1, 2008)

We report experimental evidences of anomalous kinetic roughening in the stable displacement of an oil–air interface in a Hele–Shaw cell with strong quenched disorder. The disorder consists on a random modulation of the gap spacing transverse to the growth direction (tracks). We have performed experiments varying average interface velocity and gap spacing, and measured the scaling exponents. We have obtained $\beta \simeq 0.50$, $\beta^* \simeq 0.25$, $\alpha \simeq 1.0$, $\alpha_{loc} \simeq 0.5$, and $z \simeq 2$. When there is no fluid injection, the interface is driven solely by capillary forces, and a higher value of β around $\beta = 0.65$ is measured. The presence of multiscaling and the particular morphology of the interfaces, characterized by high slopes that follow a Lévy distribution, confirms the existence of anomalous scaling. From a detailed study of the motion of the oil–air interface we show that the anomaly is a consequence of different local velocities over tracks plus the coupling in the motion between neighboring tracks. The anomaly disappears at high interface velocities, weak capillary forces, or when the disorder is not sufficiently persistent in the growth direction. We have also observed the absence of scaling when the disorder is very strong or when a regular modulation of the gap spacing is introduced.

PACS numbers: 47.55.Mh, 68.35.Ct, 05.40.-a

I. INTRODUCTION

The study of the morphology and dynamics of rough surfaces and interfaces in disordered media has been a subject of much interest in last years [1], and is an active field of research with relevance in technological applications and material characterization. These surfaces or interfaces are usually self–affine, i.e. statistically invariant under an anisotropic scale transformation. In many cases, the interfacial fluctuations follow the dynamic scaling of Family–Vicsek (FV) [2], which allows a description of the scaling properties of the interfacial fluctuations in terms of a growth exponent β, a roughness exponent α, and a dynamic exponent z. However, many growth models [3, 4, 5, 6, 7, 8], experiments of fracture on brittle materials, such as rock [9] or wood [10, 11, 12], as well as experiments on sputtering [13], molecular beam epitaxy [14], and electrodeposition [15] have shown that the FV scaling is limited, and a new ansatz, known as *anomalous scaling* [7, 16, 17], must be introduced. The particularity of the anomalous scaling is that local and global interfacial fluctuations scale in a different way, so in general the global growth and roughness exponents, β and α respectively, differ from the local ones β^* and α_{loc}.

In experiments of fracture on brittle materials, while α is clearly dependent on the material and the fracture mode, the measured exponents α_{loc} seem to have a universal value, in the range $\alpha_{loc}^{3D} = 0.8 - 0.9$ for three–dimensional fractures, and $\alpha_{loc}^{2D} = 0.6 - 0.7$ for two–dimensional fractures. López *et al.* [9] reported $\alpha = 1.2$ in an experiment of fracture in a granite block, while in fracture of wood Morel *et al.* [10] obtained $\alpha = 1.60$ and $\alpha = 1.35$ for two different wood specimens. In these experiments they also obtained $\beta = 0.26$ and $\beta^* = 0.14$. An interesting observation from the experiments of fracture in wood, where tangential and radial fractures were studied [12], is that the morphology of the interfaces for the former were characterized by large slopes, in contrast with the smoother appearance of the latter. As pointed out by López *et al.* [9], the origin of anomalous scaling in these experiments seems to be related with these large slopes in the morphology of the interfaces.

In a previous work [19] we presented an experimental study of forced fluid invasion in a Hele-Shaw cell with quenched disorder. We focused on the limit of weak capillary forces, and studied different types of disorder configurations at different interface velocities and gap spacings. The results obtained showed that the interfacial fluctuations scaled with time through a growth exponent $\beta \simeq 0.50$, which was almost independent of the experimental parameters. The values of the roughness exponents were characterized by two regimes, α_1 at short length scales and α_2 at long length scales. For high interface velocities, we obtained $\alpha_1 \simeq 1.3$ and $\alpha_2 \simeq 0$, independently of the disorder configuration. For moderate and low velocities, however, different values were obtained depending on the disorder configuration, and different scaling regimes were reported. In addition, when the disorder was totally persistent in the direction of growth, and for sufficiently strong capillary forces, a new regime emerged. This new regime must be described in the framework of anomalous scaling and was discussed in a recent Letter [20]. We obtained the scaling exponents for a specific set of experimental parameters, and explored the range of validity of the anomaly. We also in-

troduced a phenomenological model that reproduces the interface dynamics observed experimentally and the scaling exponents.

The objective of the present paper is to analyze the experimental evidences of anomalous scaling in a systematic way, introducing additional techniques for the detection of anomalous scaling, such as multiscaling and the statistical distribution of slopes. The experimental range of anomalous scaling is studied in depth, and we investigate the effects of average interface velocity, gap spacing, and disorder configuration. We also consider the situation in which the interface is solely driven by capillary forces, which allows understanding better the behavior of the interface at the scale of the disorder and its relation with the scaling exponents in particular limits of the experiments.

The outline of the paper is as follows. In Sec. II we review the Family-Vicsek and the anomalous scaling ansatzs. In Sec. III we introduce the experimental setup, and in Sec. IV we describe the methodology used in data analysis. The main experimental results are presented and analyzed in Sec. V. The discussion and final conclusions are given in Section VI.

II. SCALING ANSATZS

A. Family-Vicsek scaling

The statistical properties of a one–dimensional interface defined by a function $h(x,t)$ (interface height at position x and time t) are usually described in terms of the fluctuations of h. The *global* width in a system of lateral size L is defined as $w(L,t) = \langle [h(x,t) - \tilde{h}(t)]^2 \rangle_x^{1/2}$, where x is the position, $\tilde{h}(t) = \langle h(x,t) \rangle_x$, and $<>_x$ is an spatial average in the x direction. In the dynamic scaling assumption of Family-Vicsek (FV) [2], $w(L,t)$ scales as

$$w(L,t) = L^\alpha f(L/t^{1/z}), \qquad (1)$$

where z is the dynamical exponent and $f(u)$ the scaling function

$$f(u) \sim \begin{cases} \text{const} & \text{if} \quad u \ll 1, \\ u^{-\alpha} & \text{if} \quad u \gg 1. \end{cases} \qquad (2)$$

Here α is the roughness exponent and characterizes the scaling of the surface at saturation, $w(L, t \gg L^z) \sim L^\alpha$. L^z characterizes the saturation time, $t_\times \sim L^z$. It is customary to introduce a growth exponent β, which characterizes the growth of the interfacial fluctuations before saturation, $w(L, t \ll L^z) \sim t^\beta$. The exponents α, β, and z verify the scaling relation $\alpha = z\beta$.

An important feature of the FV assumption is that the scaling behavior of the surface can also be obtained by looking at the *local* width over a window of size $l \ll L$. The scaling is then

$$w(l,t) \sim \begin{cases} t^\beta & \text{if} \quad t \ll l^z, \\ l^\alpha & \text{if} \quad t \gg l^z. \end{cases} \qquad (3)$$

The roughness exponent α can also be obtained by studying the power spectrum of the interfacial fluctuations, $S(k,t) = \langle H(k,t)H(-k,t) \rangle$, where $H(k,t) = \sum_x [h(x,t) - \tilde{h}(t)] \exp(ikx)$. In the FV assumption, the power spectrum scales as

$$S(k,t) = k^{-(2\alpha+1)} s(kt^{1/z}), \qquad (4)$$

where s is the scaling function

$$s(u) \sim \begin{cases} u^{2\alpha+1} & \text{if} \quad u \ll 1, \\ \text{const} & \text{if} \quad u \gg 1. \end{cases} \qquad (5)$$

B. Anomalous scaling

As mentioned in the introduction, experimental results and several growth models that do not follow the FV dynamic scaling have led to the introduction of a new, more general dynamic scaling hypothesis known as *anomalous scaling* [7, 16, 17]. The origin of this new scaling comes from the different behavior of global and local interfacial fluctuations. While the global width scales as in the FV scaling, the local width follows a different scaling given by

$$w(l,t) \sim \begin{cases} t^\beta & \text{if} \quad t \ll l^z, \\ l^{\alpha_{loc}} t^{\beta^*} & \text{if} \quad l^z \ll t \ll L^z, \\ l^{\alpha_{loc}} L^{\alpha-\alpha_{loc}} & \text{if} \quad L^z \ll t, \end{cases} \qquad (6)$$

where $\beta^* = (\alpha - \alpha_{loc})/z$ is the local, anomalous growth exponent, and α_{loc} the local roughness exponent. It is common to define $\theta = \alpha - \alpha_{loc}$ as the *anomalous exponent*, which measures the degree of anomaly [16, 17]. Therefore, in the case of anomalous scaling, two more scaling exponents β^* and α_{loc} are needed to characterize the scaling behaviour of the surface. When $\theta = 0$ and $\beta^* = 0$ local and global scales behave in the same way, and we recover the usual FV scaling.

It is common to define a scaling function for the behavior of $w(l,t)$, defining $g(u)$ as $g(l/t^{1/z}) = w(l,t)/l^\alpha$. From Eq. (6), $g(u)$ is expected to scale as

$$g(u) \sim \begin{cases} u^{-(\alpha-\alpha_{loc})} & \text{if} \quad u \ll 1, \\ u^{-\alpha} & \text{if} \quad u \gg 1. \end{cases} \qquad (7)$$

One of the implications of the anomalous scaling is that the local width saturates when the system size saturates as well, i.e. at times $t_\times$, and *not* at the local time $t_l \sim l^z$ as occurs in the FV scaling. It is also interesting to notice that the anomalous scaling can be identified in an experiment by plotting the local width $w(l,t)$ as a function of time for different window sizes. According to Eq. (6) the different curves would show a vertical shift proportional to $l^{\alpha_{loc}}$.

In terms of the power spectrum, Eq. (4), the anomalous scaling follows a new scaling function $s(u)$ given by

$$s(u) \sim \begin{cases} u^{2\alpha+1} & \text{if} \quad u \ll 1, \\ u^{2\theta} & \text{if} \quad u \gg 1. \end{cases} \qquad (8)$$
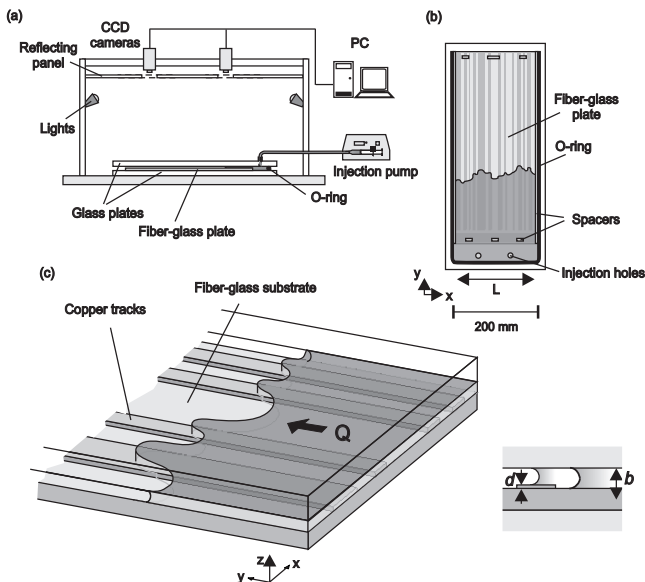
FIG. 1: Sketch of the experimental setup. a) Side view. b) Top view. c) Schematic representation of the oil–air interface and the disorder pattern.

For times $t \gg t_\times$ the power spectrum scales as $S(k,t) \sim k^{-(2\alpha_{loc}+1)}t^{2\theta/z}$ and not simply as $k^{-(2\alpha+1)}$ of the ordinary scaling.

In general, it is usual to differentiate between two types of anomalous scaling: *super-roughness* and *intrinsic anomalous scaling*. Super-roughness is characterized by $\alpha_{loc} = 1$ and $\alpha > 1$, although the structure factor follows the ordinary scaling given by Eqs. (4) and (5). Thus, for super-roughness, the power spectrum provides information about the global roughness exponent α. The intrinsic anomalous scaling follows strictly the scaling given by the scaling function of Eq. (8). This implies that the decay of the power spectrum with k gives only a measure of α_{loc}, not of α. Moreover, the particular temporal dependence of the scaling of the power spectrum allows identifying the existence of intrinsic anomalous scaling by the presence of a vertical shift of the spectral curves at different times. One has to be cautious with this particularity, because the observation of a vertical shift, however, does not imply necessarily the existence of intrinsic anomalous scaling.

The different forms of anomalous scaling are included in a generic dynamic scaling ansatz recently introduced by Ramasco *et al.* [21].

III. EXPERIMENTAL SETUP AND PROCEDURE

The experimental setup used here has been described previously in Refs. [19, 20]. The setup (Fig. 1) consists on a horizontal Hele–Shaw cell which contains a pattern of copper tracks placed over a fiberglass substrate. The tracks are d=0.06 ± 0.01 mm high and are randomly distributed along the lateral direction x without overlap, and filling 35 % of the substrate. The lateral size of the unit track is 1.50 ± 0.04 mm, but wider tracks are obtained during design when two or more unit tracks are placed one adjacent to the other. The separation between the fiberglass substrate and the top glass defines the gap spacing b, which has been varied in the range $0.16 \leq b \leq 0.75$ mm. A silicone oil (Rhodorsil 47 V) with kinematic viscosity $\nu = 50$ mm^2/s, density $\rho = 998$ kg/m^3, and surface tension oil–air $\sigma = 20.7$ mN/m at room temperature, is injected at one side of the cell, and displaces the air initially present. The evolution of the oil–air interface is monitored using 2 CCD cameras. A typical example of the morphology of an interface and its temporal evolution is shown in Fig. 2.

The oil is injected at constant volumetric injection rate Q by means of a syringe pump. The presence of the disorder, however, makes the cell inhomogeneous in the z direction, so that Q is not exactly proportional to the average interface velocity v measured on the images. Nevertheless, since the free gap $b - d$ is always comparable to the total gap b, the *two–dimensional* interface velocity v is still well characterized. On the other hand, to make the comparison between different experiments easy, we will measure v in terms of a reference velocity $V = 0.04$ mm/s.

Although the disorder made of tracks (which will be called T 1.50, the numeric value indicating the width of the unit track in mm) has been the main disorder pattern used in the experiments, other disorder configurations have been used. These configurations are characterized by a random distribution of squares with a lateral size of 1.50 or 0.40 mm, and will be called SQ 1.50 and SQ 0.40 respectively. A full description and characterization of these disorders, plus more detailed information about the experimental setup and procedure can be found in Ref. [19].

IV. DATA TREATMENT

As explained in Sec. II, we study the roughening process of the interfaces through the interfacial *rms* width $w(l,t)$ and the power spectrum $S(k,t)$. The profile $h(x,t)$, obtained from the analysis of the images, contains 515 points corresponding to a lateral size of 190 mm. Because the oil tends to advance at the side walls of the cell, we have a distorsion of the front that penetrates a distance p from each side wall. This penetration length depends on average interface velocity and is spe-
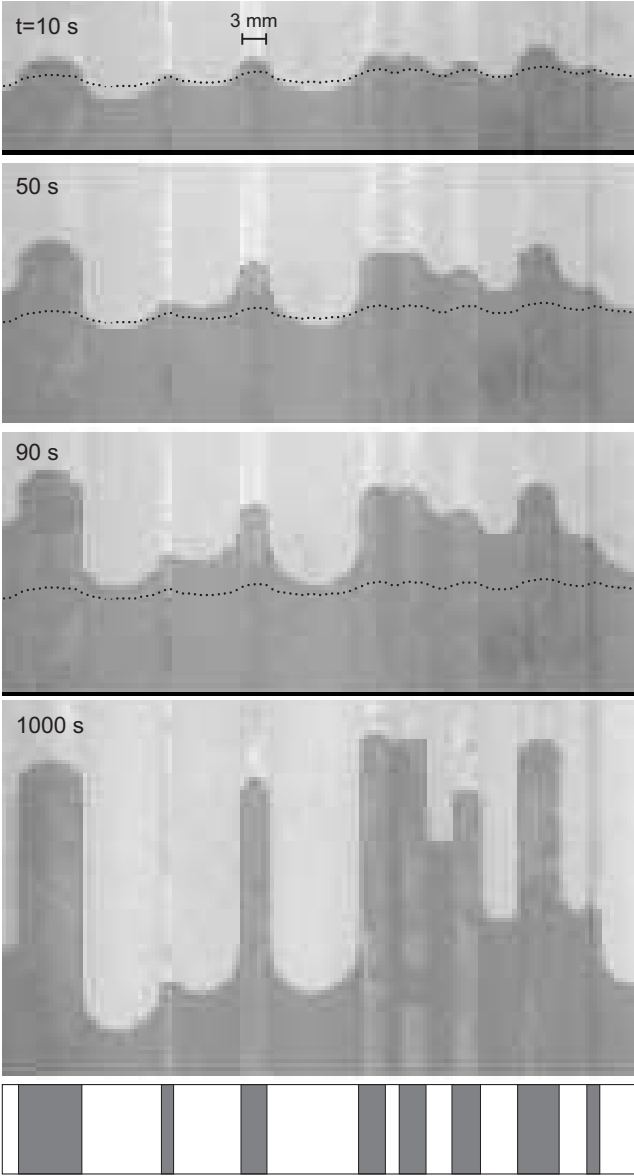
FIG. 2: Close-up views of the oil–air interface with disorder T 1.50. The first three pictures are early stages, while the last one corresponds to saturation. The position of the copper tracks is shown in the bottom box. The dotted line shows the position and shape of the interface profile at $t = 0$ s. The experimental parameters are $v = 0.08$ mm/s, $b = 0.36$ mm.
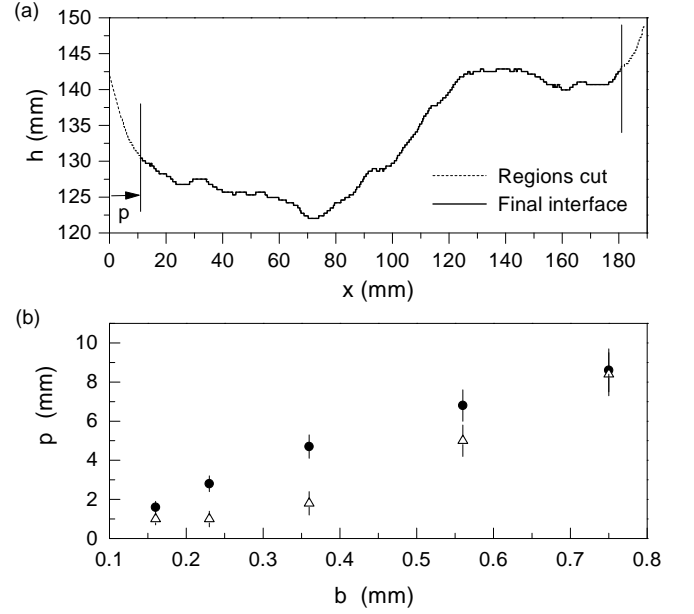

FIG. 3: (a) Example of an interface with strong side wall distortions. The dashed lines represent the regions cut at the end of the interface, and the solid line the interface finally studied. The experimental parameters are $v = 0.08$ mm/s, $b = 0.75$ mm and disorder SQ 1.50. (b) Penetration length p as a function of the gap spacing b for SQ 1.50 (dots) and T 1.50 (triangles).

cially sensitive to variations in gap spacing. An example is presented in Fig. 3(a), which shows the effect of the distortion on an interface with experimental parameters $v = 0.08$ mm/s, $b = 0.75$ mm and disorder SQ 1.50. To evaluate the effect of the distortion, we have measured the penetration length p at different gap spacings b for two disorder configurations, SQ 1.50 and T 1.50. The results are presented in Fig. 3(b), and show that p in-

creases quickly with gap spacing. For $b = 0.75$ mm, the largest value studied, p is about 8 mm. Notice also that the presence of a columnar disorder reduces significantly the effect of the distortion for the smallest gap spacings. To minimize the effect of the distortion we have cut 8 mm from both ends of all interfaces, as shown in Fig. 3(a), reducing them to a final lateral size of 174 mm (470 pixels). For data analysis convenience (particularly in the computation of the power spectrum), we have extended the number of points to 512 using linear interpolation. Finally, we have forced periodic boundary conditions by subtracting the straight line that connects the two ends of the interface. This procedure, well documented in the literature of kinetic roughening [22], eliminates an artificial overall slope -2 in the power spectrum due to the discontinuity at the two ends [23].

Because the initial stages of roughening are so fast, the interface profile at $t = 0$ s is not a flat interface, but a profile with an initial roughness $w(0)$, as can be observed in Fig. 2. This roughness, on one hand, does not permit to observe the growth of the small scales at short times; on the other, $w(0)$ is different from one disorder configuration to another, which makes the early stages strongly dependent on the particular realization of the disorder. To eliminate these effects, we will always plot the *subtracted width* $W(l,t)$, defined as $W(l,t) = \langle w^2(l,t) - w^2(l,0) \rangle^{1/2}$,

where the brackets indicate average over disorder realizations. This correction is an standard procedure in the field of growing interfaces, and is reported in both experiments and numerical simulations [1, 13, 24].

Another aspect of interest concerning the analysis of our experimental data is the various methods available in the literature to obtain the growth and roughness exponents. In this work we have obtained the growth exponents β and β^* through the scaling of $W(l,t)$ with time. We have also used an alternative way to measure β^*, proposed by López [18], in which the growth of the mean local slopes, $\rho(t) = \langle \overline{(\nabla h)^2} \rangle^{1/2}$, is analyzed. Usually $\rho(t)$ scales with time as $\rho(t) \sim t^\kappa$, with $\kappa < 0$ for the ordinary scaling and $\kappa > 0$ for anomalous scaling. In this last case, κ is identified with the local growth exponent β^*. The local roughness exponents α_{loc} have been obtained through the analysis of the power spectrum $S(k,t)$. The results obtained have been checked using other methods, such as the dependency of the height-height correlation function $C(l,t)$ or $W(l,t)$ with the *window* size l, in both cases scaling as $l^{\alpha_{loc}}$. We have obtained, within error bars, similar results to those from $S(k,t)$. Finally, in the framework of intrinsic anomalous scaling, the only direct way to measure the global roughness exponents α, and in addition $z = \alpha/\beta$, is through the analysis of $C(L,t)$ or $W(L,t)$ with the *system* size L. Both quantities scale as L^α. Because it is not practical to perform experiments varying the system size, we have not measured global roughness exponents directly. Instead, they have been obtained from the collapse of $S(k,t)$ or $W(l,t)$. Notice that information about the value of α is contained in both the vertical displacement of the spectral curves with time (Eqs. (4) and (8)) and the vertical shift of the $W(l,t)$ curves for different window sizes (Eq. (6)). The error bars that we give in the final numeric value of an specific scaling exponent takes into account the various methods of analysis and the error in the different collapses.

V. EXPERIMENTAL RESULTS AND ANALYSIS

A. Evidence of anomalous scaling

The first evidence of anomalous scaling in these experiments was presented in our previous work [20] and corresponded to the experimental parameters $v = 0.08$ mm/s ($2V$) and $b = 0.36$ mm. Here, for completeness, we will show similar experimental results for a different set of parameters, namely $v = 0.04$ mm/s (V) and $b = 0.36$ mm.

1. Interfacial width

Fig. 4(a) shows the results obtained for $W(l,t)$ for progressively smaller window sizes. We obtain clear exponents $\beta = 0.52 \pm 0.04$ (corresponding to $l = L$) and
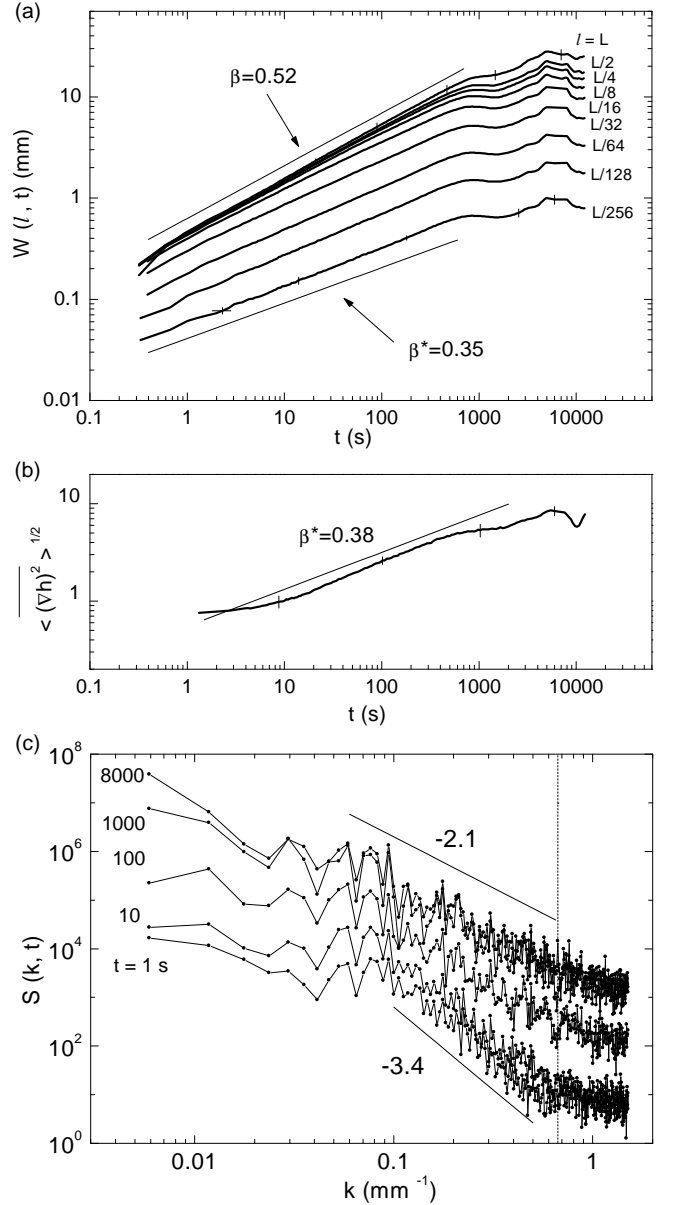

FIG. 4: Experimental results for $b = 0.36$ mm, $v = 0.04$ mm/s (V) and disorder T 1.50. a) Analysis of $W(l,t)$ for different window sizes. b) Analysis of the mean local slopes as a function of time. c) Temporal evolution of the power spectrum. The vertical line in c) indicates the spatial scale of the disorder.

$\beta^* = 0.35 \pm 0.05$ (for $l = L/256$). The fact that β^* is clearly different from zero is a robust evidence of anomalous scaling. Moreover, the behavior of the different curves is in good agreement with the anomalous scaling ansatz of Eq. (6), i.e. the plots for different window sizes are vertically shifted. Notice also that the saturation takes place at $t_\times$ (the saturation time of the full

system) for all window sizes.

2. Local slopes

To check the reliability of the exponent β^* we have also studied the scaling of the mean local slopes with time. The result is presented in Fig. 4(b), obtaining $\beta^* = 0.38 \pm 0.05$, in agreement with the result of β^* using $W(l = L/256, t)$.

3. Power spectrum

The analysis of the interfacial fluctuations through the power spectrum is presented in Fig. 4(c). The first important observation is that the spectral curves are shifted vertically, the shift being maximum at short times, reducing progressively as time increases, and disappearing at saturation ($t = t_\times \simeq 2000$ s). The presence of this vertical displacement of the spectral curves is a signature of anomalous scaling. The evolution of the power spectrum gives two clear power law dependencies, at short times with slope -3.4 ± 0.1, and at saturation with slope -2.1 ± 0.1. The former is a transient regime whose origin is the strong dominance of the capillary forces at very short times. The latter provides the local roughness exponent, $\alpha_{loc} = 0.55 \pm 0.10$ in this case.

To get the values of α and z we have collapsed the plots of Fig. 4(c) in accordance with the scaling function of Eq. (8), i.e. plotting $S(k,t)k^{2\alpha+1}$ as a function of $kt^{1/z}$. This collapse, shown in Fig. 5(a), refines the numerical values of the experimental results and gives the values of α and z. We obtain in this way:

$$\beta = 0.50 \pm 0.04, \ \beta^* = 0.30 \pm 0.04,$$
$$\alpha = 1.1 \pm 0.1, \ \alpha_{loc} = 0.5 \pm 0.1, \ z = 2.2 \pm 0.2. \quad (9)$$

An alternative collapse that confirms the validity of these results can be performed using the scaling function defined in Eq. (7). This collapse is shown in Fig. 5(b).

4. Multiscaling

The presence of anomalous scaling can also be identified by checking for multiscaling [4]. For this purpose, we have studied the scaling of the generalized correlations of order q, of the form $C_q(l) = \{\langle (h(x+l,t) - h(x,t))^q \rangle\}^{1/q} \sim l^{\alpha_q}$, where α_q are local roughness exponents. The results obtained are shown in Fig. 6, which gives the values of α_q at different orders q. We get a progressive decrease of the measured exponent, varying from $\alpha_2 \simeq 0.55$ to $\alpha_6 \simeq 0.22$, which confirms the existence of multiscaling in the experiment and, therefore, of anomalous scaling.
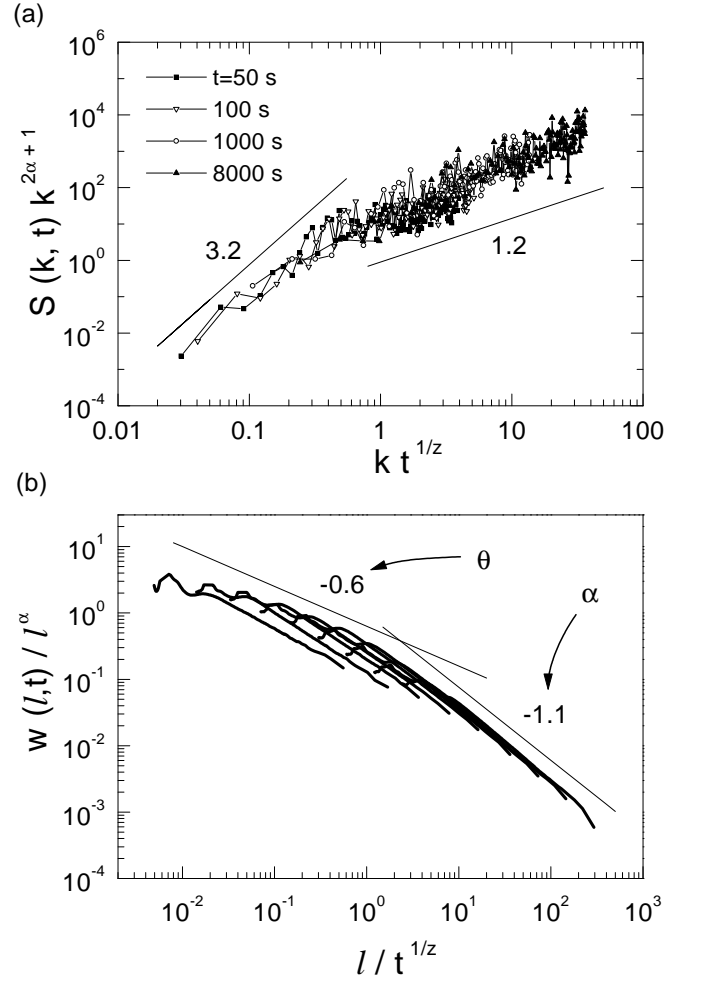

FIG. 5: a) Collapse of the power spectrum of Fig. 4(c) for $t > 10$ s using the scaling function of Eq. (8). b) Collapse of the $W(l,t)$ plots of Fig. 4(a), using the scaling function of Eq. (7).

B. Experimental range of anomalous scaling

Once the existence of anomalous scaling is well characterized for a specific set of experimental parameters, we are now interested in analyzing the range of validity of the anomaly. We have performed a series of experiments varying v and fixing the gap spacing to $b = 0.36$ mm and, on the other hand, a series of experiments varying b and fixing the average interface velocity to $v = 0.08$ mm/s (2V). Because we can identify the existence of anomalous scaling by looking at the behavior of the smallest scales, i.e. the existence of a $\beta^* \neq 0$, we present the results by plotting the local growth exponent β^* for the different experiments.
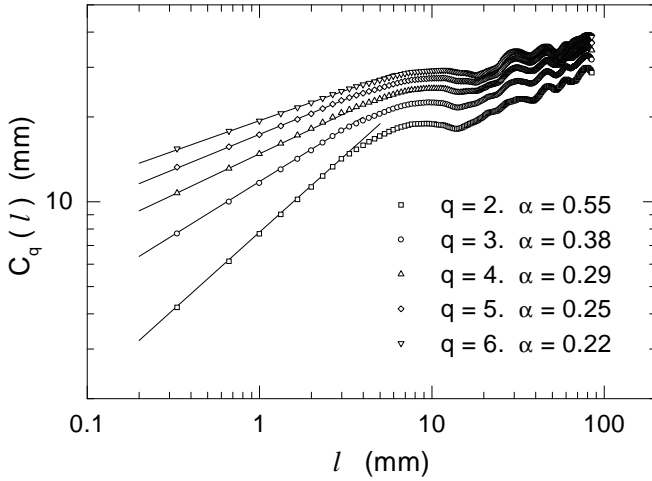
FIG. 6: Multiscaling analysis through the computation of the q–order height-height correlation function for interfaces at saturation. The experimental parameters are $v = 0.04$ mm/s, $b = 0.36$ mm and disorder T 1.50.
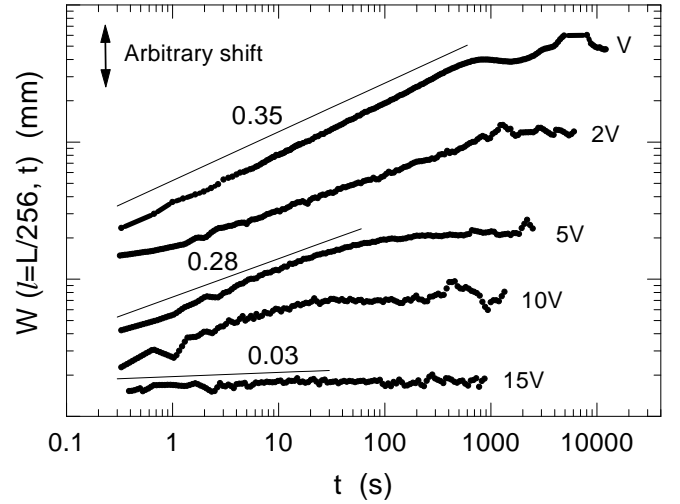

FIG. 7: W(t) curves for a window size $l = L/256$ and different interface velocities. The gap spacing is $b = 0.36$ mm in all cases, and $V = 0.04$ mm/s. The curves are vertically shifted for clarity.

1. Interface velocity

The results of β^* at different v are presented in Fig. 7. In a wide range of interface velocities, from V to $10\,V$, the measured exponent β^* is robust and not very sensitive to changes in the velocity, varying from 0.35 ± 0.04 for velocity V to 0.28 ± 0.04 for velocity $10\,V$. For velocities $v \gtrsim 15V$, however, the measured value of β^* quickly decays to a value close to zero, indicating that over a threshold velocity (about $13V$ for $b = 0.36$ mm) the anomaly disappears.

In terms of the power spectrum, when the velocity is varied from V to $15V$, we always observe a vertical shift of the spectral curves, and the power spectrum at different times can be collapsed to get the set of scaling exponents. Above the previous threshold velocity, the power spectrum follows the ordinary scaling, i.e. without vertical displacement.

2. Gap spacing

The results of β^* at different b are presented in Fig. 8. It is clear from the different plots that the exponent β^* is rather sensitive to variations of the gap spacing. Three different behaviors can be observed: i) For *small* values of b (around $b = 0.16$ mm), where capillary forces are dominant, we get $\beta^* = 0.52 \pm 0.04$, which is identical to the corresponding value of β. This similitude is discussed in Sec. V E. ii) For *moderate* values of b (in the range $0.23 \le b \le 0.56$ mm) we get values of β^* that vary from 0.35 ± 0.05 for $b = 0.23$ mm to 0.25 ± 0.04 for $b = 0.56$ mm. This range of gap spacings is character-

ized by strong (but not dominant) capillary forces, and is the region where the anomalous scaling can be fully characterized. iii) For *large* values of b ($b \gtrsim 0.60$ mm) we get $\beta^* = 0.10 \pm 0.04$ for $b = 0.75$ mm, and β^* is nearly zero for larger gap spacings. In this regime capillary forces are not sufficiently strong, and the anomalous scaling disappears. The analysis of β^* through the scaling of the mean local slopes has given identical results within error bars, although the sensitivity of this analysis to short–time transients makes it less reliable.

Concerning the power spectrum, in the range $0.23 \le b \le 0.56$, the vertical shift of the spectral curves is present, and a regime characterized by anomalous scaling can be described. For $b = 0.16$ mm, although the spectral curves are vertically shifted, an scaling regime is not identifiable at all. The power spectra can be collapsed, but not reliable α, α_{loc}, and z exponents can be obtained. For $b \gtrsim 0.6$ mm, a vertical shift in the power spectra is not observed, and the scaling of the interfacial fluctuations is best described in the framework of ordinary scaling.

3. Disorder properties

Other modifications that we have carried out to study the range of validity of the anomalous scaling are the track width and the persistence of the disorder along the growth direction. Fig. 9 shows the variation of the local interfacial fluctuations for four different disorder configurations. The gap spacing and velocity have been fixed to $b = 0.36$ mm and $v = 2V$ respectively. For T 0.40
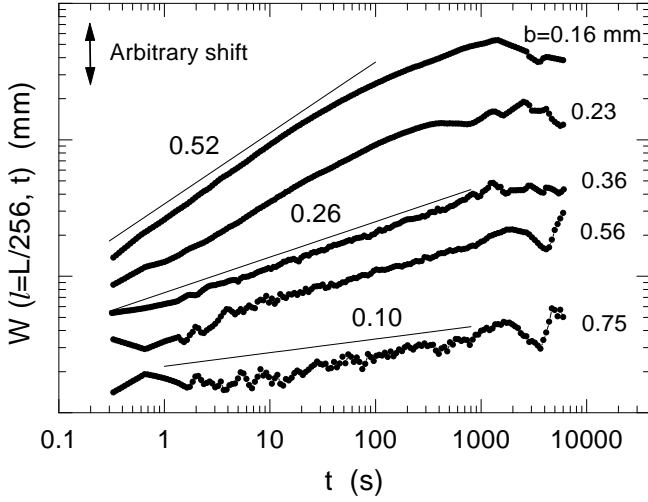
FIG. 8: W(t) curves for a window size $l = L/256$ and different gap spacings. The interface velocity is $v = 2V = 0.08$ mm/s in all cases. The curves are vertically shifted for clarity.

FIG. 9: W(t) curves for a window size $l = L/256$ and different disorder configurations with progressively shorter persistence in the growth direction. $b = 0.36$ mm and $v = 2V = 0.08$ mm/s in all cases. The curves are vertically shifted for clarity.

we get a similar result from that obtained with T 1.50, measuring $\beta^* = 0.29 \pm 0.05$. However, we have evidences that the anomaly decreases as we reduce the width of the basic track, and it disappears when the width of the basic track is $\lesssim 0.20$ mm, due to the fact that the in–plane curvature over the copper track becomes similar to the curvature in the z direction.

Next, we study different disorder configurations with progressively smaller persistence in the growth direction. For SQ 1.50, although the saturation time for the full system is at $t_\times \simeq 1000$ s, we observe that the local interfacial fluctuations saturate at much shorter time, which is more characteristic of the ordinary scaling. However, we still observe traces of anomalous scaling at early times, for which $\beta^* = 0.26 \pm 0.04$. This is somehow not surprising taking into account that, for this disorder, the first array of squares is equivalent to T 1.50, but only 1.50 mm long. Thus, at very short times, the growth follows the same behavior as tracks. With a driving velocity 0.08 mm/s, the interface takes about $10 - 20$ s in crossing the first array of squares, which is the same time for which we observe the presence of anomalous scaling. For SQ 0.40, with $t_\times \simeq 300$ s, we measure $\beta^* = 0.05 \pm 0.04$, which is indicative of the absence of anomalous scaling.

4. Characterization by the statistical distributions of slopes

We have also considered an alternative analysis to confirm the results of anomalous scaling. In a recent work, Asikainen *et al.* [26] showed that the presence of anomalous scaling can be associated to the presence of multiscaling on one hand, and to high slopes in the morphology
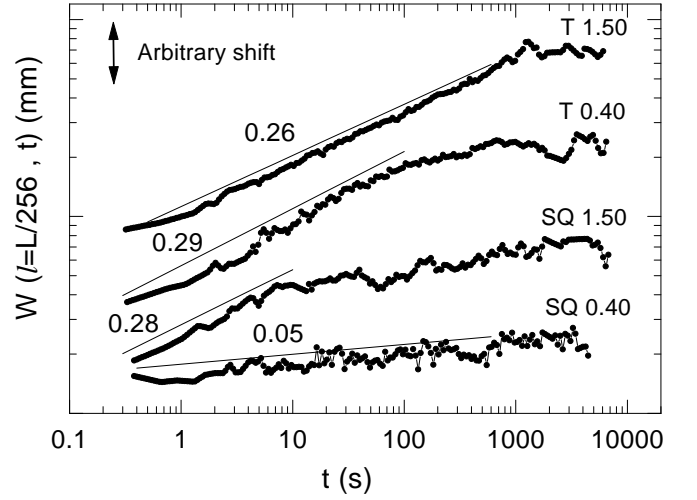
of the interfaces on the other. According to these authors, the distribution function of these slopes, $P(\Delta h)$, with $\Delta h \equiv |h(x_{i+1} - h_x|$, scales following a Lévy distribution, $P(\Delta h) \sim \Delta h^{-\gamma}$, where $0 < \gamma < 2$; while for ordinary scaling $P(\Delta h)$ follows a Gaussian distribution. We have checked this prediction with our experimental results. Fig. 10(a) compares the shape of three different interfaces with different degrees of anomalous scaling. In all cases $v = 2V$ and $b = 0.36$ mm. All the interfaces are in the saturation regime. For T 1.50 (the case most representative of anomalous scaling) the interface presents high slopes at the edges of the copper tracks. For T 0.40 some regions present high slopes, but in general the interface looks smoother. This case shows anomalous scaling, but the degree of the anomaly is much weaker than the previous case. For SQ 1.50 the interface is very smooth and the interfacial fluctuations are best described with the FV scaling, with only traces of anomalous scaling at very short times. The interfaces in these three cases are similar to those reported in fracture of wood by Engøy *et al.* in Fig. 1 of Ref. [12]. In particular, the interfaces for T 1.50 or T 0.40 look like interfaces obtained from tangential fracture in wood, both characterized by high slopes and anomalous scaling. In the same line, the interfaces for SQ 1.50 are similar to those obtained from radial fracture. These similitudes indicate that the role of the wood fibers is probably equivalent to the role of the copper tracks in our system as the origin of the anomalous scaling.

The distribution functions for the different interface morphologies are shown in Fig. 10(b) and (c). For T 1.50 we have two different regimes. Up to $\Delta h \simeq 2$ mm

(dashed line in the plot) we have the contribution of the slopes corresponding to the structure inside tracks. For $\Delta h > 2$ mm (solid line), the contribution to the distribution function arises from the edges of the tracks. This last contribution is the one responsible for the anomalous scaling, and scales with Δh with an exponent -0.6 ± 0.1. A similar result is observed for T 0.40. In this case, if we do not consider the contribution of the structure inside tracks (up to 1 mm), we get a power law dependency with exponent -2.0 ± 0.2. The fact that the anomaly is weaker for T 0.40 compared to T 1.50 is illustrated in this case by the larger value of the slope. If we compare the distribution functions of T 1.50 and SQ 1.50 we observe that, in the latter case, there is contribution only from small slopes. $P(\Delta h)$ would scale in this case with an exponent -3.6, far from the values expect for anomalous scaling.

C. Experiments at Q=0

In order to understand the origin of the anomalous scaling, the previous results indicate that a more detailed investigation about the role of the capillary forces at the scale of the disorder has to be carried out. For this reason we have performed experiments at $Q = 0$, where interfacial growth is driven solely by capillary forces.

The experiments at $Q = 0$ have been performed by initially driving the interface at high velocity until it has reached the center of the cell. Then the pump is stopped and the experiment started. We have investigated five gap spacings, in the range $0.16 \le b \le 0.75$ mm, and characterized the interface velocity over copper tracks and fiberglass channels. For sufficiently small gap spacing, up to $b \simeq 0.36$ mm, the morphology of the interface adopts a finger–like configuration, which ultimately causes that the interface pinches–off at long times. For this reason we have reduced the duration of the experiments to 500 s for all gap spacings.

Fig. 11 shows a comparison of the interfaces at the end of the experiments with different gap spacings. The horizontal line represents the average position of the interface at $t = 0$. For $b = 0.16$ mm the points of the interface over the different tracks move almost independently, with weak coupling between neighboring tracks: the oil over copper tracks always advances, while the oil over fiberglass channels, except for some particular locations, always recedes, driven by the different capillary forces associated with the different curvature of the meniscii over copper tracks and fiberglass substrate. As we increase the gap spacing, the coupling in the motion of the interface over neighboring tracks is progressively more intense. For $b = 0.36$ mm the advance over a specific copper track is coupled with its neighbors. The oil advances or recedes in a given track or channel depending on the particular realization of the disorder. Only the widest copper tracks or fiberglass channels have an independent motion. For $b = 0.56$ mm the coupling reaches larger regions of the
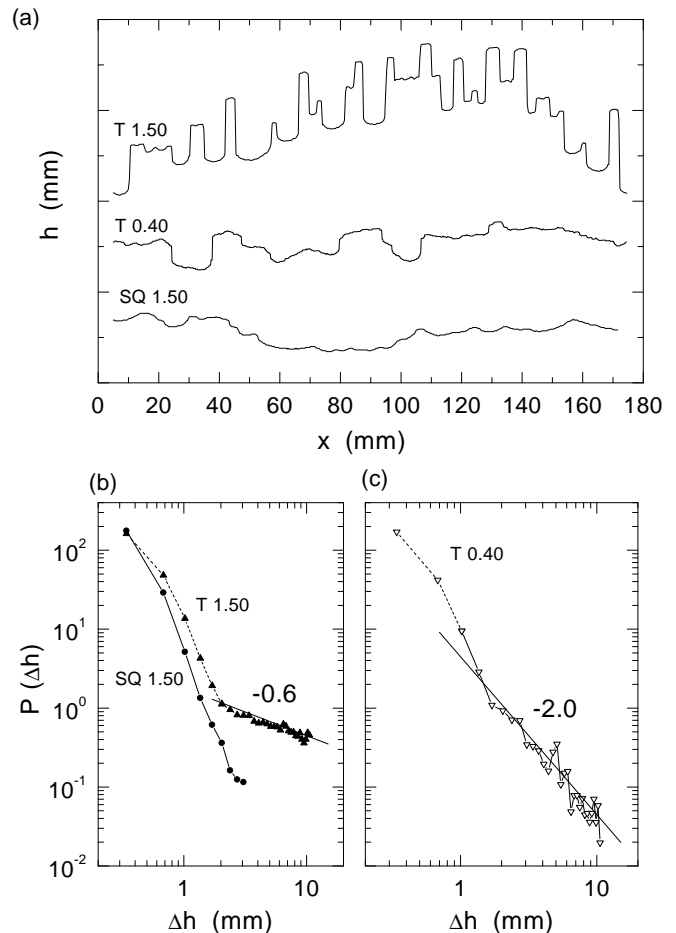

FIG. 10: (a) Samples of interfaces for different disorder configurations and identical experimental parameters $v = 0.08$ mm/s and $b = 0.36$ mm. (b) Distribution function $P(\Delta h)$, with $\Delta h \equiv |h(x_{i+1} - h_x|$, for local slopes, comparing T 1.50 and SQ 1.50. (c) The same for T 0.40. See text for details of the power law fits.

cell, and for $b = 0.75$ the capillary forces are not longer sufficient to allow a large deformation of the interface.

It is also noticeable that the average position of the interface does not keep at rest. Indeed, it advances in the same direction as the oil over copper tracks. This is a consequence of the three-dimensional nature of the experiment. The total mass of fluid in the cell is conserved, but not the area measured on the images. However, the measured velocity of advance of the interface is very low. For $b = 0.36$ mm, for example, the velocity is about $V/10$.

The first analysis that we have performed with the experiments at $Q = 0$ is studying the growth of interfacial fluctuations with time. Fig. 12 shows the $W(t)$ curves for four different gap spacings. We observe power laws with a growth exponent β that decreases from 0.65 ± 0.04 for $b = 0.16$ mm to 0.50 ± 0.04 for $b = 0.75$ mm. Clearly, when
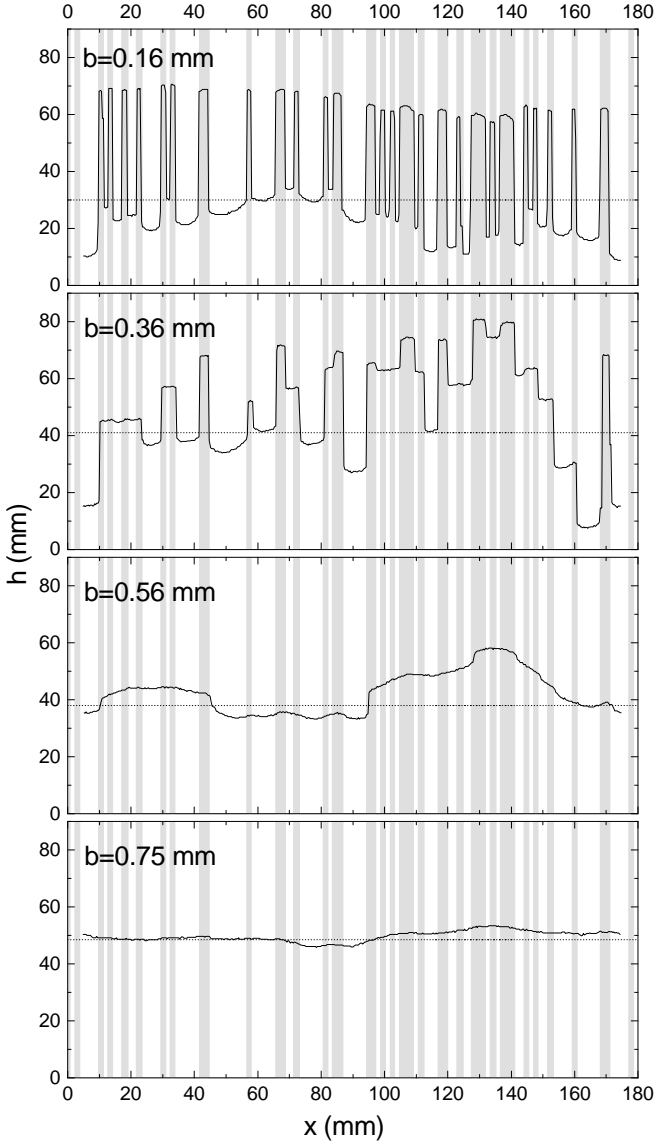
FIG. 11: Example of interfaces at $Q = 0$ with different gap spacings and disorder T 1.50 mm. All the interfaces correspond to $t = 500$ s. The horizontal dotted line indicates the position of the interface at $t = 0$ s.

FIG. 12: Log-log plot of $W(t)$ for experiments at $Q = 0$ with four different gap spacings and disorder T 1.50 mm. The straight line with slope 0.65 corresponds to a fit of the experiments with $b = 0.16$ mm and 0.36 mm. The straight line with slope 0.50 is a fit to the experiment with $b = 0.75$ mm. Each curve is an average over two disorder realizations, with one run per disorder realization.

the capillary forces are sufficiently strong to allow for both the advance of the oil over tracks and the recession of the oil over fiberglass channels, we get a larger value of the growth exponent than in all other cases. The same behavior is observed for β^*, varying from 0.65 ± 0.04 for $b = 0.16$ mm to 0.15 ± 0.05 for $b = 0.75$ mm.

Concerning the behavior of the power spectrum, the fact that the experiments do not reach a saturation regime makes the analysis of the power spectrum incomplete. Qualitatively, we have observed a vertical shift 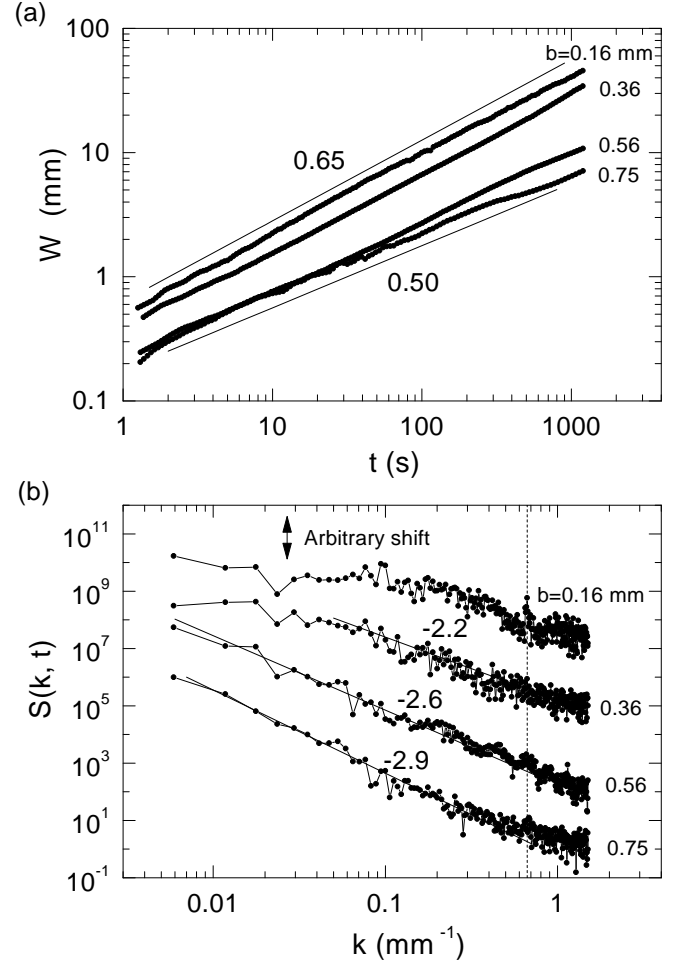of the spectral curves as time increases for gap spacings up to $b = 0.56$ mm. For $b = 0.75$ mm the vertical shift is not present, confirming the absence of anomalous scaling for values of $b \geq 0.60$ mm for any interface velocity.

The second analysis that we have performed has been a detailed study of the motion of the interface over copper tracks or fiberglass channels separately. In Fig. 13 we represent the variation of the mean height $< h >$ for points of the interface that are advancing over copper tracks. For gap spacings in the range $0.16 \leq b \leq 0.36$ mm, the mean height is a power law of time with an exponent 0.50 ± 0.03. For larger gap spacings, the exponent is progressively smaller, and reaches 0.32 ± 0.03 for $b = 0.75$ mm. We have hints that the exponent tends to zero as the capillary forces become even weaker. A sim-
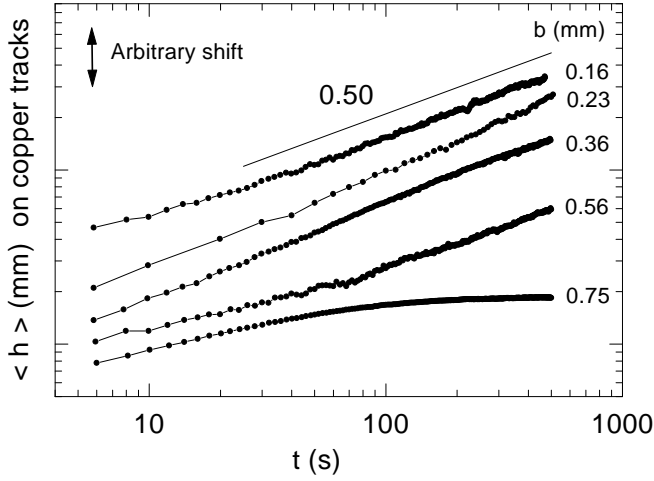
FIG. 13: Log-log plot of the average height as a function of time for the interface points advancing over copper tracks, for different gap spacings. $Q = 0$ in all cases. The curves are vertically shifted for clarity.

ilar analysis can be carried out for the fiberglass channels. In this case we get the same behavior in the range $0.16 \leq b \leq 0.36$ mm, with an exponent 0.50 ± 0.03. For $b \geq 0.60$ mm not clear scaling can be identified. Finally, we have also studied the motion on individual tracks, in order to know the role of track width. Considering tracks whose motion is not coupled with its neighbors we have obtained that tracks of different width show the same behavior $< h > \sim t^{0.5}$, but the different curves are displaced a factor proportional to the track width.

From these studies we conclude that it is possible to describe the motion over a single copper track, v_+^i, or fiberglass channel, v_-^i, by the simple law

$$v_{\pm}^i(t) = A_{\pm}^i(b, D_{\pm}^i)\, t^{-1/2} \qquad \text{for} \qquad t \geqslant 1 \text{ s}, \qquad (10)$$

where $A_{\pm}^i(b, D_{\pm}^i)$ is a prefactor that depends on the gap spacing b and the individual track or channel width D^i. Averaging out the prefactor $A_{\pm}^i$ over different track or channel widths we obtain a characteristic maximum velocity $v_{M\pm}$ for a given gap spacing. Eq. (10) becomes now

$$v_{\pm}(t) = v_{M\pm}(b)\, t^{-1/2} \qquad \text{for} \qquad t \geqslant 1 \text{ s}. \qquad (11)$$

In general $v_{M_+} > v_{M_-}$ due to the different gap spacing on copper tracks and on fiberglass channels. This difference, however, is progressively smaller as b increases. For $b \geq 0.36$ mm it is reasonable to consider $v_{M_+} \simeq v_{M_-} \equiv v_M$. The time $t = 1$ s, determined from systematic experimental observations, is a typical time in which the velocity jumps from the average interface velocity out of the disorder to v_M inside the disorder.

D. From $Q = 0$ to low injection rates

Eq. (11) gives the velocity over copper tracks or fiberglass channels when $Q = 0$ (no injection). In the presence of injection, when the interface is driven at an average interface velocity $v \neq 0$, the behavior observed experimentally is modified in the form

$$v_{\pm}(t) = v \pm (v_M - v)\, t^{-1/2}, \qquad (12)$$

where $v_M = v_M(b)$ and v_+ and v_- are the velocities averaged over copper tracks and fiberglass channels respectively. Thus, when the interface gets in contact with the disorder, the velocity on copper tracks jumps to a maximum v_M in a characteristic time of 1 s and then relaxes as $t^{-1/2}$ to the nominal velocity. On fiberglass channels, the velocity is zero or even negative at short times, and as time goes on, the velocity increases until it reaches the nominal velocity at long times. Fig. 2 illustrates this behavior. At short times, $t \simeq 10$ s, all the oil over copper tracks is advancing, while the oil on the widest fiberglass channels is receding. At $t \simeq 50$ s the oil on fiberglass channels has stopped receding. At later times, the velocity on different points of the interface tends asymptotically to the nominal velocity, reached at saturation.

At low injection rates, the external velocity v can be tuned appropriately to have an initial regime in which the oil advances over copper tracks and recedes over fiberglass channels, followed by a regime in which the oil advances at all points of the interface. This leads to two scaling regimes for $W(l, t)$, at short times with a growth exponent $\simeq 0.65$, which corresponds to a regime dominated by strong capillary forces, and at longer times with a growth exponent $\simeq 0.50$, which corresponds to a regime where capillary and viscous forces are better balanced. We have illustrated this behavior by performing experiments at low v. In particular, we have studied velocities $V/2$ and $V/10$ using a gap spacing $b = 0.36$ mm and disorder T 1.50. The results are presented in Fig. 14. The difficulty of these experiments is that the interface pinches–off before it reaches saturation, so we can investigate only the growth regime. For $V/2$ we observe the two power law regimes described before. For $V/10$, only the first regime can be observed before the interface breaks. These results are qualitatively in agreement with the analysis of Hernández-Machado *et al.* [25], who predicted two scaling regimes, $\beta_1 = 5/6$ at short times (surface tension in the plane dominant) and $\beta_2 = 1/2$ at long times (viscous pressure dominant). However, the presence of anomalous scaling and the complicated role of capillary forces in our experiments makes it difficult a direct comparison with the predictions of Hernández-Machado *et al.*.

Another result than can be obtained from Eq. (12) is a prediction for the saturation time $t_\times$ as a function of the average interface velocity v. We can estimate $t_\times$ for a given v and gap spacing b by considering that saturation takes place when all tracks reach the nominal velocity
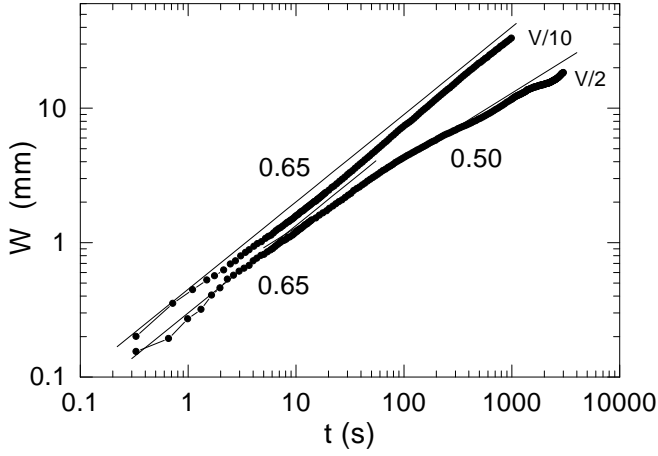
FIG. 14: log-log plot of $W(t)$ for experiments at low velocity with disorder T 1.50 mm. The end of the experiments is the moment at which the interfaces pinch–off. The gap spacing is $b = 0.36$ mm. Each curve is an average over two disorder configurations, with one run per disorder configuration.

FIG. 15: Prediction of the dependency of $t_\times$ with v. Main plot: for a given average velocity v, the system saturates when the average velocity on copper tracks decays to v. Inset: a log-log plot of the $t_\times$ obtained by the previous method (filled dots) as a function of v gives a straight line with slope -2. The triangles are the experimental results for T 1.50 and $b = 0.36$ mm.

v. This is not strictly exact due to the coupling between neighboring tracks, but it gives a good estimate of the dependency $t_\times(v)$, as shown in Fig. 15. For a given experiment with velocity $v_i < v_M$ the saturation takes place when the function $v_M\, t^{-1/2}$ crosses the nominal velocity. Thus, as shown in the inset of the figure, $t_\times$ is expected to scale as $t_\times \sim v^{-2}$. This result is confirmed by our experiments with disorder T 1.50 and $b = 0.36$ mm (open triangles in the inset).

E. Experiments with a regular modulation of the gap spacing

In order to analyze the importance of the coupling between neighboring tracks, we have performed experiments with a regular modulation of the gap spacing, consisting on copper tracks 6 mm wide separated by fiber-glass channels 6 mm wide. Interface velocity and gap spacing are set to $v = 0.08$ mm/s and $b = 0.36$ mm respectively. The regular modulation and the temporal evolution of the resulting interfaces are presented in Fig. 16(a). Due to the symmetry of the regular pattern there is no growing correlation length along the direction of the interface. For this reason, a dynamic scaling of the interfacial fluctuations cannot even be defined. The growth of the interfacial width is due to the independent, equivalent growth of interface fingers over copper tracks, which follow the $t^{-1/2}$ behavior (Eq. 12). The system saturates when the fingers reach the nominal velocity. This is shown in Fig. 16(b), which shows the evolution of $W(l,t)$ for the global ($l = L$) and local ($l = L/256$) scales. The figure reveals that both scales grow in the same way. The
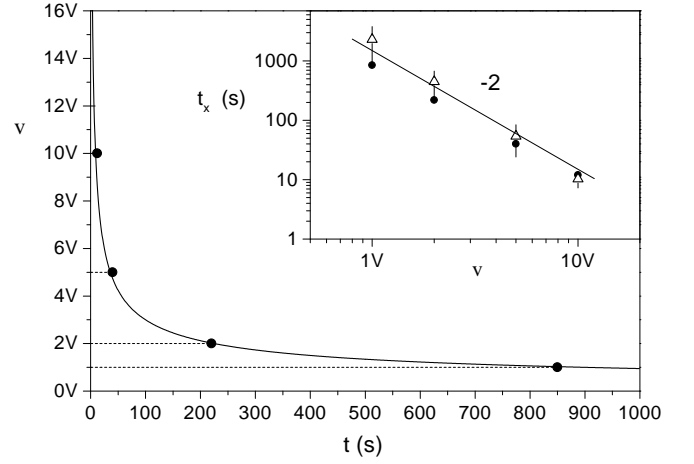
absence of dynamic scaling is also confirmed by the power spectrum, shown in Fig. 16(c). We obtain a nearly flat spectrum, with a large peak at the value of k that corresponds to the spatial periodicity of the underlying regular pattern. We also observe a vertical shift of the spectra at different times, caused by the progressive elongation of the oil fingers over copper tracks during growth.

The previous experiments with a regular modulation of the gap spacing illustrate the need of a growing correlation length along the interface to reach a dynamic scaling regime. Similarly to these experiments, the lateral growth of the correlation length can also be inhibited when the modulation of the gap spacing is random, provided that the experimental parameters are such that the motion over tracks is not coupled and, on each track, follows Eq. (12). Thus, for very small gap spacings ($b \leq 0.16$ mm) and $v \geq V$ we observe a growth of the interfacial width with exponent $\simeq 0.5$ for both global and local scales. Similarly, in the experiments at $Q = 0$ with $b = 0.16$ mm the same exponent $\simeq 0.65$ is measured for both global and local scales. The power spectrum of this case also demonstrates the lack of dynamic scaling, as can be seen in the top plot of Fig. 12(b). When the modulation of the gap spacing is regular, the transition to saturation is sharp due to the fact that all tracks have the same width, and thus all the oil fingers reach the nominal velocity at the same time. For a random pattern the transition to saturation is smooth, and does not take place strictly until the widest copper tracks (those that have the highest value of A_+^i) reach the nominal velocity. The plot for $b = 0.16$ mm of Fig. 8 illustrates this
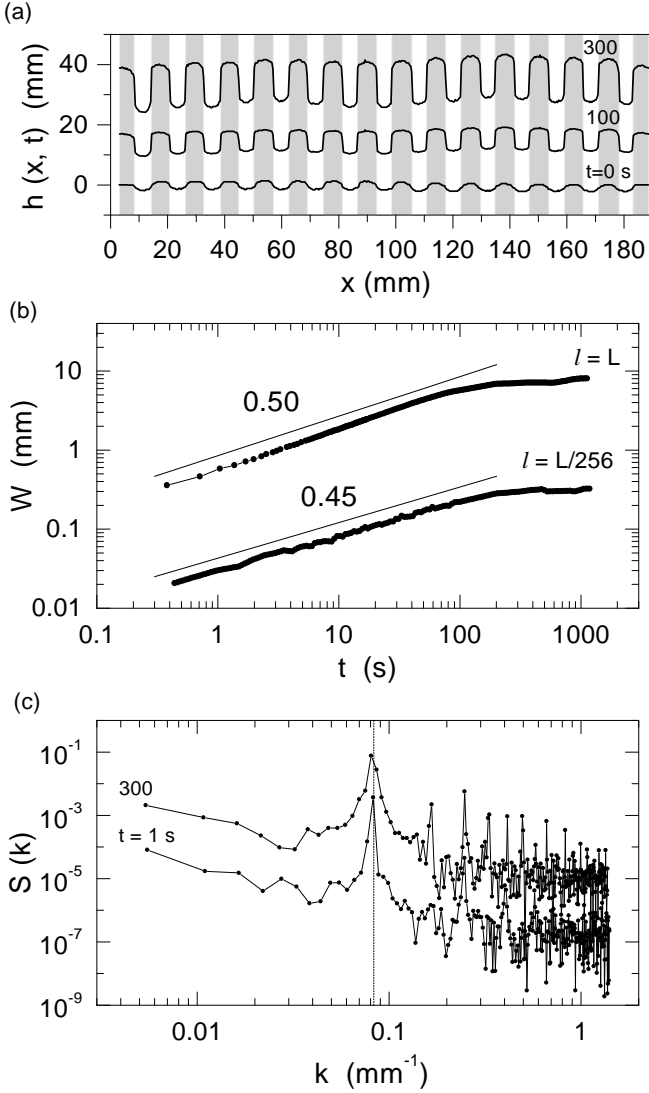
FIG. 16: Experiments with a regular modulation of the gap spacing, using tracks 6 mm wide. The experimental parameters are $v = 2V = 0.08$ mm/s and $b = 0.36$ mm. (a) Temporal evolution of the interfaces. (b) $W(l,t)$ plots for global $(l = L)$ and local $(l = L/256)$ scales. (c) Power spectrum at saturation $(t = 300$ s$)$. The vertical line indicates the k corresponding to the spatial periodicity of the regular pattern.

behavior.

VI. DISCUSSION AND CONCLUSIONS

Our experimental results show that two ingredients are necessary to observe anomalous scaling in a disordered Hele–Shaw cell: i) strong destabilizing capillary forces, sufficiently persistent in the direction of growth, and ii) coupling in the motion between neighboring tracks.

These two ingredients give rise to sharp slopes at the track edges together with a growing correlation length along the interface. This scenario is represented in the phase diagram of Fig. 17, which shows the different regions of scaling explored experimentally. Each point of the diagram is an average over 6 experiments (3 disorder configurations and 2 runs per disorder configuration). The dark grey area represents the region where an anomalous scaling has been identified. We have indicated the value of $2\theta/z$, which is the value needed to collapse vertically the spectral curves and, therefore, indicates the degree of anomaly. For $0.15 \leq b \leq 0.60$ mm, and for driving velocities below $v_M(b)$, the capillary forces are strong enough to allow an initial acceleration and subsequent deceleration of the oil fingers over copper tracks, but sufficiently weak to allow coupling between neighboring tracks. For $v > v_M$, the viscous forces become dominant, and the anomalous scaling is unobservable. For $b > 0.60$ mm, the capillary forces are not sufficiently strong and we have ordinary scaling for any velocity. Finally, for $b \leq 0.15$ mm (light grey area in Fig. 17), the capillary forces are dominant, and the oil fingers over copper tracks and fiberglass channels have independent motion. In this situation a dynamic scaling scenario is not adequate because there is no growing correlation length along the interface. Although $W(l,t)$ grows as a power law of time, this is a consequence of the independent behavior on each track given by Eq. (11). Although it is not possible to determine the scaling exponents, still is possible to perform a vertical collapse of the spectral curves because only the *difference* between α and α_{loc} (i.e. θ) is needed. This allows to give the values of $2\theta/z$ for $b = 0.16$ mm.

In conclusion, we have reported experiments of anomalous kinetic roughening in Hele–Shaw flows with quenched disorder. We have studied the displacement of an oil–air interface for different strength of the capillary forces, flow velocity, and disorder configurations. We have observed that the scaling of the interfacial fluctuations follows the intrinsic anomalous scaling ansatz in conditions of sufficiently strong capillary forces, low velocities, and a persistent disorder in the growth direction. A random distribution of tracks has been used as representative of a persistent disorder. A different scaling for the global and local interfacial fluctuations has been measured, with exponents $\beta \simeq 0.50$, $\beta^* \simeq 0.25$, $\alpha \simeq 1.0$, $\alpha_{loc} \simeq 0.5$, and $z \simeq 2$. The presence of anomalous scaling has been confirmed by the existence of multiscaling. When capillary forces become dominant or when a regular track pattern is used, however, there is no growing correlation length along the interface, and therefore no dynamic scaling. A detailed investigation of the interface dynamics at the scale of the disorder shows that the anomaly is a consequence of the different velocities over copper tracks and fiberglass channels plus the coupled motion between neighboring tracks. The resulting dynamics gives interface profiles characterized by high slopes at the edges of the copper tracks. These slopes
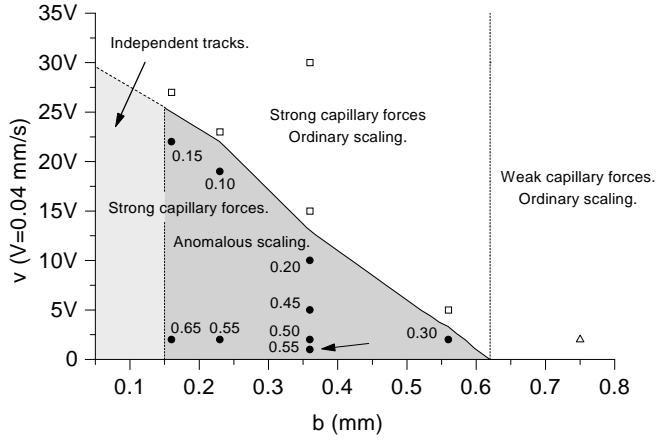
FIG. 17: Phase diagram for the anomalous scaling. The symbols indicate the parameters explored experimentally. The numbers beside the symbols in the anomalous scaling region give the value of $2\theta/z$. The solid line represents the curve $v = v_M(b)$. The arrow indicates the particular experiment of Figs. 4 and 5.

follow an anomalous Lévy distribution characteristic of systems which display anomalous scaling.

VII.   ACKNOWLEDGEMENTS

[1] A.-L. Barabási and H.E. Stanley, *Fractal Concepts in Surface Growth*, Cambridge University Press, Cambridge (1995).

[2] F. Family and T. Vicsek, J. Phys. A **18**, L75 (1985).

[3] M. Schroeder *et al.*, Europhys. Lett. **24**, 563 (1993)

[4] J. Krug, Phys. Rev. Lett. **72**, 2907 (1994).

[5] S. Das Sarma *et al.*, Phys. Rev. E **53**, 359 (1996)

[6] C. Dasgupta, S. Das Sarma, and J.M. Kim, Phys. Rev. E **54**, R4552 (1996)

[7] J.M. López and M.A. Rodríguez, Phys. Rev. E **54**, R2189 (1996)

[8] M. Castro *et al.*, Phys. Rev. E **57**, R2491 (1998)

[9] J.M. López and J. Schmittbuhl, Phys. Rev. E **57**, 6405 (1998).

[10] S. Morel, J. Schmittbuhl, J.M. López, and G. Valentin, Phys. Rev. E **58**, 6999 (1998).

[11] S. Morel, J. Schmittbuhl, E. Bouchaud, and G. Valentin, Phys. Rev. Lett. **85**, 1678 (2000).

[12] T. Engøy, K. J. Måløy, A. Hansen, and S. Roux, Phys. Rev. Lett. **73**, 834 (1994).

[13] J.H. Jeffries, J.-K. Zuo, and M.M. Craig, Phys. Rev. Lett. **76**, 4931 (1996).

[14] H.-N. Yang, G.-C. Wang, and T.-M. Lu, Phys. Rev. Lett. **73**, 2348 (1994).

[15] S. Huo and W. Schwarzacher, Phys. Rev. Lett. **86**, 256 (2001).

[16] J.M. López, M.A. Rodríguez, and R. Cuerno, Phys. Rev. E **56**, 3993 (1997)

[17] J.M. López, M.A. Rodríguez, and R. Cuerno, Physica A **246**, 329 (1997).

[18] J. M. López. Phys. Rev. Lett. 83, 4594 (1999).

[19] J. Soriano, J. Ortín, and A. Hernández-Machado, Phys. Rev. E., in press (2002).

[20] J. Soriano, J.J. Ramasco, M.A. Rodríguez, A. Hernández-Machado, and J. Ortín, Phys. Rev. Lett. **89**, 026102 (2002).

[21] J.J. Ramasco, J.M. López, and M.A. Rodríguez, Phys. Rev. Lett. **84**, 2199 (2000).

[22] I. Simonsen, A. Hansen, and O. M. Nes, Phys. Rev. E **58**, 2779 (1998).

[23] J. Schmittbuhl, J.-P. Vilotte, and S. Roux, Phys. Rev. E **51**, 131 (1995).

[24] G. Tripathy and W. van Saarloos, Phys. Rev. Lett. **85**, 3556 (2000).

[25] A. Hernández–Machado, J. Soriano, A.M. Lacasta, M.A. Rodríguez, L. Ramírez–Piscina, and J. Ortín, Europhys. Lett. **55**, 194 (2001).

[26] J. Asikainen, S. Majaniemi, M. Dubé, and T. Ala-Nissila, Phys. Rev. E. **65**, 052104 (2002).